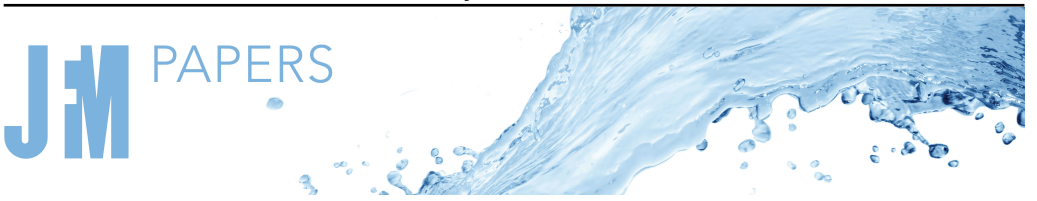
J. Fluid Mech. (2025), *vol.* 1015, A13, doi:10.1017/jfm.2025.10336



Angstrom-scale ionic streaming when the electrical double-layer concept fails

Jiajia Lu[1], **Shuyong Luan**[2], **Shenghui Guo**[1], **Libing Duan**[1], **Guanghua Du**[3] and **Yanbo Xie**[2]

[1]School of Physical Science and Technology, Northwestern Polytechnical University, Xi'an 710072, PR China

[2]National Key Laboratory of Aircraft Configuration Design, School of Aeronautics and Institute of Extreme Mechanics, Northwestern Polytechnical University, Xi'an 710072, PR China

[3]Institute of Modern Physics, Chinese Academy of Sciences, Lanzhou 730000, PR China

Corresponding author: Yanbo Xie, ybxie@nwpu.edu.cn

(Received 26 August 2024; revised 19 May 2025; accepted 4 June 2025)

A knowledge gap exists for flows and transport phenomena at the angstrom scale when the Poisson–Nernst–Planck equation based on the concept of the electrical double layer fails. We discovered that streaming conductance becomes pressure-dependent in angstrom channels using latent-track membranes. The streaming current emerges only when the applied pressure exceeds a threshold value, which is inconsistent with the existing knowledge as a constant. With increasing channel size, we found that the pressure-dependent streaming conductance phenomenon weakens and vanishes into a constant streaming conductance regime when the mean channel radius exceeds $\sim$2 nm. The effective surface potential derived from the streaming conductance that divides conduction anomalously increases as the channel narrows. We suspect that the pressure-dependent streaming current is due to the reinforced Coulomb interaction between counterions and deprotonated carboxyl groups at the surface, which is close to the ion channel but different from that of electrified two-dimensional materials. The streaming current emerged due to hydrodynamic friction when the counterions were released from the surface. We approximated the stochastic process of counterion dissociation by a one-dimensional Kramer escape theory framework and defined the Damköhler number to describe the transition from the nonlinear streaming conductance regime to the linear regime as functions of applied pressure and channel radius and well explained the enhanced effective surface potential in confinement.

Key words: electrokinetic flows, non-continuum effects, channel flow

© The Author(s), 2025. Published by Cambridge University Press.

https://doi.org/10.1017/jfm.2025.10336 Published online by Cambridge University Press

1. Introduction

The flow of water through an electrified surface generates a net ionic current known as streaming current (van der Heyden *et al.* 2005; Bocquet & Charlaix 2010; Xu, Yan & Xie 2024), which is one of the fundamental electrokinetic phenomena. The study of streaming current is useful in both fundamental research, such as zeta potential characterisation (Werner, Zimmermann & Kratzmüller 2001; Zimmermann, Dukhin & Werner 2001; Lyklema 2003; van der Heyden *et al.* 2006; Delgado *et al.* 2007; Storey & Bazant 2012; Siria *et al.* 2013; Emmerich *et al.* 2022), and applications like energy conversions (Olthuis *et al.* 2005; Xue *et al.* 2017; Marcotte *et al.* 2020; Alkhadra *et al.* 2022). Downscaling the channel size benefits the energy conversion by ion-layering effects (Gillespie *et al.* 2011; Gillespie 2012) and enhances the efficiency up to 50 % in Nafion systems (Catalano & Bentien 2014; Østedgaard-Munck *et al.* 2017) and power density to $\sim$25 mW m^{-2} in Mxene membranes (Yang *et al.* 2022).

The knowledge of electrokinetic phenomena and electrical double-layer theory is still developing. For instance, ion–ion interactions, typically ignored in classical double-layer theories, become critical in high-concentration or divalent electrolyte solutions, named the ionic correlation effect, which precisely describes the electrokinetic phenomena (Storey & Bazant 2012; Hartkamp *et al.* 2018; McEldrew *et al.* 2018). Besides, considering the dynamic response of ions under an external field, the description of electrokinetic phenomena is more accurate than the static double-layer theories (Bazant & Squires 2004, 2010).

However, the concept of the double layer fails when the critical size of the channel comes to the regime of a single hydrated ion, where only a few water molecules exist in the cross-section of the channel. New technologies and emerging two-dimensional materials enable us to study flows and mass transport at the molecular level (Wang *et al.* 2017; Faucher *et al.* 2019; Aluru *et al.* 2023). Numerical findings demonstrated that the flow and transport phenomena were inconsistent with the classical understandings such as those of ultrafast water flows (Holt *et al.* 2006; Radha *et al.* 2016; Keerthi *et al.* 2021; Itoh *et al.* 2022), voltage-induced mobility change (Esfandiar *et al.* 2017), anomalous dielectric constant (Bonthuis & Netz 2012; Fumagalli *et al.* 2018), ionic Coulomb blockade (Feng *et al.* 2016; Kavokine *et al.* 2019; Cao *et al.* 2024), breakdown of the Nernst–Einstein relation (Li *et al.* 2023), quantum friction (Kavokine, Bocquet & Bocquet 2022) and fluidic memristors (Robin *et al.* 2021, 2023; Shi *et al.* 2023), indicating that underlying new physics still need to be revealed.

Compared with voltage-driven ionic transport, the streaming current in angstrom channels was rarely studied in experiments since previous work was conducted on two-dimensional materials that were either charge-free (Zhou *et al.* 2023) or homogeneously charged by voltage gating (Marcotte *et al.* 2020) or plasma activation (Emmerich *et al.* 2022). Mouterde *et al.* (2019) successfully enhanced the molecular streaming current up to 20 times by voltage gating on carbon nanotubes. Their results showed the ionic mobility derived from the streaming current shows strong nonlinear effects as gating voltage rises, opening a new route to control ion transport. In contrast to non-gated channels, where the streaming conductance grows linearly with applied pressure, voltage gating induces a Péclet-dependent conductance that results in a nonlinear streaming current (Marcotte *et al.* 2020). Keerthi *et al.* (2021) studied the molecular streaming in angstrom slits and discovered the very large difference in slip length between graphene and hexagonal boron nitride surfaces, revealing that the electrokinetic mobility of ions increases with the salt concentration and the slipping surface.

However, for most dielectric materials, such as biological ion channels, the surface acquires charges due to dissociation or adsorption of protons or charged species at functional groups (Behrens & Grier 2001; Noskov, Berneche & Roux 2004; Li *et al.* 2019;

https://doi.org/10.1017/jfm.2025.10336 Published online by Cambridge University Press

Tan *et al.* 2020). Thus, the classical electric double-layer theory is not applicable as we have to consider the discrete charged sites in angstrom confinement. In classical colloid science, deprotonated surfaces are typically modelled with a homogeneous surface charge, as the relevant length scales (usually >100 nm) far exceed the spacing between charged sites (site densities less than $\sim 1\,\mathrm{nm}^{-2}$). However, under angstrom-scale confinement, surface charges become discrete. For example, a 10 nm long channel with a diameter of 1 nm and a surface charge density of $-5\ \mathrm{m\,C\,m}^{-2}$ contains only one charged site, with most surface atoms remaining neutral. In this regime, classical electric double-layer theory breaks down, and the discrete nature of charged sites must be explicitly considered, where charge distribution may significantly impact the flow (Xie *et al.* 2020) and ionic transport in confinement (Kim & Netz 2006; Kavokine *et al.* 2019; Xie *et al.* 2023). Thus, the electrokinetic phenomena are still unclear in angstrom channels when the double-layer concept fails.

In this work, we investigated the streaming conductance of charged latent-track angstrom channels. We found that in angstrom-scale latent-track channels, the streaming current emerges when the applied pressure exceeds a threshold value and represents a strong nonlinear increasing feature as pressure increases, inconsistent with the existing understanding of the streaming conductance known as a constant (van der Heyden *et al.* 2005). However, as the diameter increased, the nonlinear feature of streaming conductance gradually weakened and eventually vanished, becoming pressure-independent as described by classical nanofluidic theories. We estimated the surface potential of nanochannels by streaming conductance divided by conduction, which anomalously increases as the channel narrows when external pressure is applied to the membrane. We attributed the pressure-dependent streaming conductance to the presence of counterions bound to the surface charge when channels approach the angstrom scale. The rise in applied pressure increases the hydrodynamic friction on the counterions, increasing the probability of counterions dissociating from the surface charge and thus forming the streaming current. As the channel size increases, the Coulomb interaction between counterions and surface charge reduces, resulting in constant streaming conductance again. We approximated the pressure-dependent streaming conductance by using the one-dimensional (1-D) Kramer escape approach, which qualitatively explained the experimental observation in angstrom channels, including the impacts of applied pressure and size effects. With the defined Damköhler number, we could identify the pressure-dependent and pressure-independent regimes by a phase diagram of the dimensionless coefficient $Da/(Da+1)$. Our work provides anomalous streaming current phenomena in angstrom channels that show new features in flows and ionic transport at the smallest scale, which is possibly useful for ion separations or energy applications in the future.

2. Systems and characterisation

Figure 1(*a*) illustrates the fabrication process of latent-track membranes (Wen *et al.* 2016). A 12 μm thick polyethylene terephthalate (PET) foil was first irradiated by Kr^{+} ions with an energy of 6 MeV u^{-1} with beam density of 3×10^{8} cm^{-2} from the Lanzhou Heavy Ion Research Facility (HIRFL). Then, we irradiated both sides of each specimen under UV light (65 mW cm^{-2}) for 10 min to decompose the damaged zone along the latent track (Schauries *et al.* 2018). The photo-decomposed polymer molecules could be electrophoretically removed using 0.01 M KCl solution at 50 °C for at least half an hour, named soft etching (Wen *et al.* 2016; Apel *et al.* 2022; Guo *et al.* 2024). Once the conductance reached a saturated value, we believe all radiolysis products had been removed from the channels, resulting in the formation of 1-D angstrom-scale channels as

https://doi.org/10.1017/jfm.2025.10336 Published online by Cambridge University Press

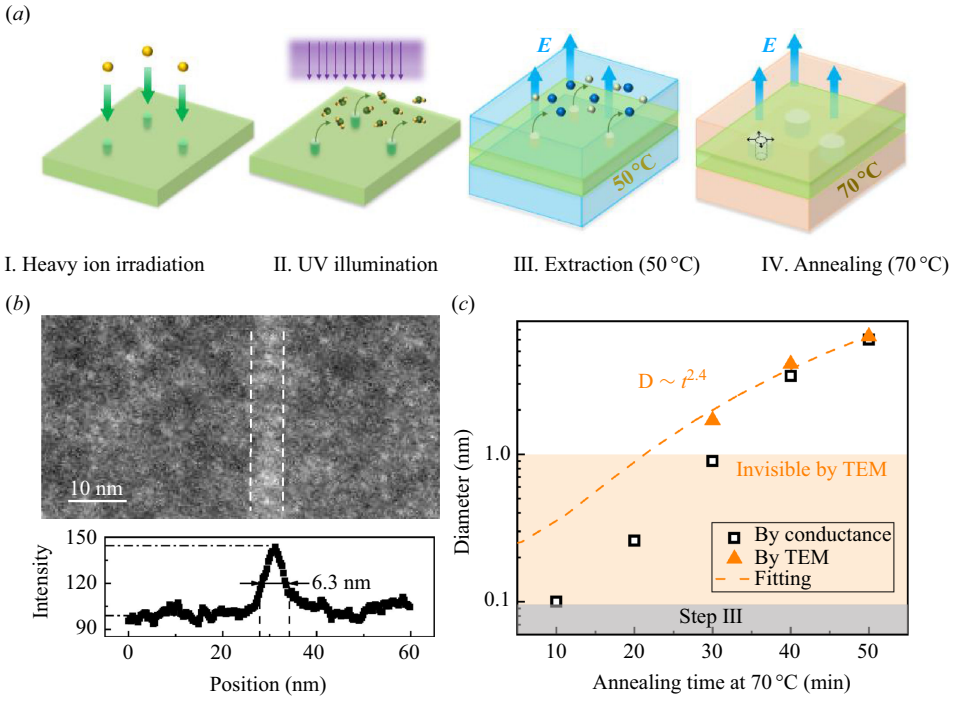


Figure 1. (*a*) The fabrication process of latent-track channels, including heavy ion irradiation (step I), UV irradiation (step II), electrophoresis to remove the radiolysis products in a 50 °C water bath (step III) and thermal annealing, if needed, in a 70 °C water bath to increase the channel size (step IV). The schemes are not to scale. (*b*) The latent-track channels stained by RuO_4 are represented as bright straight lines under TEM. We statistically measured the brightness projected onto the bottom line and took half the peak width of the brightness as the channel diameter. (*c*) The radius calculated from the measured conductance (black squares) increases with annealing time. However, only channels with diameters larger than 2 nm are visible under TEM (yellow triangles). A numerical fit (yellow dashed line) provides a reference for the channel size. Conductance measurements may underestimate channel size due to blockade effects in confinement.

we characterised by isotherm adsorptions (Xie *et al.* 2023). The membranes were well cleaned and preserved in a thermostat overnight.

To study the size effects of nanochannels, we developed the channel size by annealing latent-track channels in a water bath at 70 °C, similar to the method reported by Schauries *et al.* (2018) in air. Annealing enlarges the size of polymer nanochannels, caused by the damaged track halo diffusing into the track core (Schauries *et al.* 2018). The naming scheme of specimens is as follows: TA denotes thermal annealing, with the subsequent number indicating the temperature of the water bath (e.g. 70 represents 70 °C). The number following the dash indicates the annealing time in minutes at the given temperature. An asterisk indicates an additional specimen obtained using the same fabrication process. For example, TA70−10 refers to a specimen thermally annealed at 70 °C for 10 minutes and TA70−10* represents an additional specimen thermally annealed at 70 °C for 10 minutes. The conductance of each specimen was measured by sweeping voltage in a 0.01 M KCl solution at room temperature. However, the radius of angstrom channels can no longer be precisely characterised by the conductance, due to the strong nonlinear features (Xie *et al.* 2023). Here we take the conductance G at 10 V for later discussion, as our previous work found the calculated radius became closer to the true radius for 10 V or even higher voltage scanning due to the counterion blockade effects.

https://doi.org/10.1017/jfm.2025.10336 Published online by Cambridge University Press

Figure 1(*c*) shows that the channel diameter characterised by G at 10 V through Ohm's law is proportional to the time of annealing, where the grey area indicates the diameter characterised by the conductance after soft etching (step III) but before annealing (step IV). We found the I–V curves (figure S2 of the supplementary material available at https://doi.org/10.1017/jfm.2025.10336) gradually transition from nonlinear to linear features as the channel radius increases. Here, we characterised the latent-track nanochannels using ruthenium tetraoxide staining under transmission electron microscopy (TEM) (Adla, Fuess & Trautmann 2003). Each specimen was exposed to the vapour of RuO_4 solvent over 20 minutes to guarantee reactions with unsaturated functional groups. We embedded membranes in epoxy resin and sliced them into 100 nm sections using an ultrathin slicer (Leica UC7FC7). Each nanochannel could be recognised as a straight, bright line under electron microscopy, as shown in figure 1(*b*), due to the ruthenium dioxide deposition. We counted the average brightness of the stained region using the software DigitalMicrograph. The averaged diameter of angstrom channels based on the width at half maximum from the TEM image is shown in figure 1(*b*). The statistical results of the annealed specimen TA70−50, which stands for soft etching in a 50 °C water bath and thermal annealing at 70 °C for 50 minutes, showed that the typical width of the channel is 6.3 nm, which is almost exactly the same as the value we derived from the conductance of 6.1 nm, shown as orange symbols in figure 1(*c*).

However, as the channel size decreases to the angstrom scale, the brightness contrast in the stained area becomes apparently lower due to much fewer unsaturated functional groups. We counted the half-maximum of the brightness in TEM images, which is proportional to the amount of Ru molecules penetrating into the polymers, to predict the channel size as a dashed line shown in figure 1(*c*) (more details are provided in figure S1 of the supplementary material). We numerically fitted the diameter change as a function of annealing time t in a 70 °C water bath as $D \sim t^{2.4}$. The TEM-characterised diameter (D) matched well the calculated ones from conductance when $D > 2$ nm in the absence of nonlinear conduction. But the diameter derived from conductance starts to deviate from the dashed lines for smaller channels. The diameter calculated from the conductance is underestimated, since we found the voltage-activated conductance in latent-track channels (Xie *et al.* 2023) with the hypothesis of counterion blockade that reduces the ionic conductance conduction. The physical interpretation of the numerical fitting remains unclear, in the absence of details like the structures and dynamics of the polymers during thermal annealing. But, at least, the fitting provides a reference value for estimating the channel size, particularly in cases where both conduction measurements and TEM fail to characterise channels with diameters smaller than 2 nm. Table 1 summarises the sizes characterised using different approaches, providing a basis for analysing streaming conductance and comparing between the different methods.

3. Results and discussion

We sealed the left poly(methyl methacrylate) reservoir and clamped a piece of latent-track membrane using two polydimethylsiloxane (PDMS) gaskets, where a surface area of approximately 0.8 cm^2 of the membrane was exposed to the electrolyte solution, so that the applied pressure could be controlled from the left reservoir using a pressure pump (Fluigent) (figure 2*a*). Two Ag/AgCl electrodes were inserted in the reservoirs and connected to a Sub-femtoamp Remote SourceMeter (Keithley 6430) for current recording. Silver wires with a diameter of 0.6 mm and a length of 15 cm were polished with sandpaper for a smooth surface and rinsed with deionised water, and ultrasonically cleaned in ethanol and acetone solutions for 15 minutes to remove possible organic contamination. The

https://doi.org/10.1017/jfm.2025.10336 Published online by Cambridge University Press

Specimen	Diameter from conductance (squares) (nm)	Diameter by TEM (triangles) (nm)	Diameter from fitting (dashed line) (nm)
TA50	0.05	Invisible	0.2
TA70–10	0.1	Invisible	0.4
TA70–20	0.26	Invisible	0.9
TA70–30	0.9	1.7 (visible)	2.0
TA70–40	3.4	4.1 (visible)	3.8
TA70–50	6.0	6.3 (visible)	6.4

Table 1. Diameter of channels from calculated conductance, stained specimens under TEM and numerical fitting.

cleaned silver wires were immersed in 0.1 M $FeCl_3$ for 15 minutes to produce Ag/AgCl electrodes. The Ag/AgCl electrode area exposed to the salt solutions is approximately 1.9 cm^2 and shows a difference of a few millivolts (figure S4 of the supplementary material). We filled reservoirs with 0.01 M KCl solution at pH = 5.4, where the Debye length is ∼3 nm, which is much larger than the channel radius. A Faraday cage covered the system to reduce the noise level. We measured the streaming current from TA50 fabricated by soft etching and free of annealing, which has the smallest conduction among all specimens.

The typical I–V curve of specimen TA50 in the inset of figure 2(*d*) represents an obvious nonlinear conduction feature. We attributed the high resistance at low voltage to the strong interaction between counterions and surface charge, which may block ionic transport through the 1-D angstrom channel (Xie *et al.* 2023). Increases in applied voltage may increase the probability of counterions releasing from the surface charge, thus opening the channel for conduction. Thus, it is quite interesting to measure the streaming current in our latent-track channel, which is a 1-D charged angstrom-scale system, since the streaming current is directly proportional to the surface charge that may support the counterion blockade mechanisms. The current recordings in figure 2(*c*) show an obvious current jump from the current noise once pressure was applied at $\Delta p = 0.9$ bar, which vanished when the pressure was turned off. We take the average value of current change ΔI_1 when pressure was turned on and ΔI_2 when pressure was turned off as the streaming current, to avoid the drift of current noise due to ion concentration polarisation. The fluctuating current after the pressure was turned off was caused by mechanical vibration.

The Helmholtz–Smoluchowski (HS) equation as well as the Poisson–Nernst–Planck (PNP) equations describe the streaming current at a charged wall $I_s = \varepsilon_r \varepsilon_0 \pi R^2 \Phi \Delta p / \eta L$, where ε_r, ε_0, R, Φ, η and L are the relative permittivity of water, vacuum permittivity, channel radius, surface potential (or zeta potential in continuum regime), viscosity and channel length, as here we take the form of the HS equation for simplification. The streaming conductance defined as $S = I_s/\Delta p$ is independent of applied pressure (van der Heyden *et al.* 2005; Yaroshchuk & Luxbacher 2010; Xue *et al.* 2014): $S \sim \varepsilon_r \varepsilon_0 R^2 \Phi / \eta L$.

However, our experimental results of streaming current in latent-track angstrom channels showed a strong nonlinear feature with Δp in figure 2(*d*), which remains nearly at zero below 0.5 bar but dramatically increases as applied pressure exceeds 0.5 bar. The error bars were statistically derived from the measured streaming current in a single experiment. It seems that the streaming current can be activated by applying pressure. We suspect the pressure-dependent streaming conductance is correlated with the impacts of the angstrom channel and heterogeneous surface charge, since it was rarely found even in angstrom-scale channels, with the exception of voltage-gated Péclet-dependent conductance (Mouterde *et al.* 2019; Marcotte *et al.* 2020).

https://doi.org/10.1017/jfm.2025.10336 Published online by Cambridge University Press

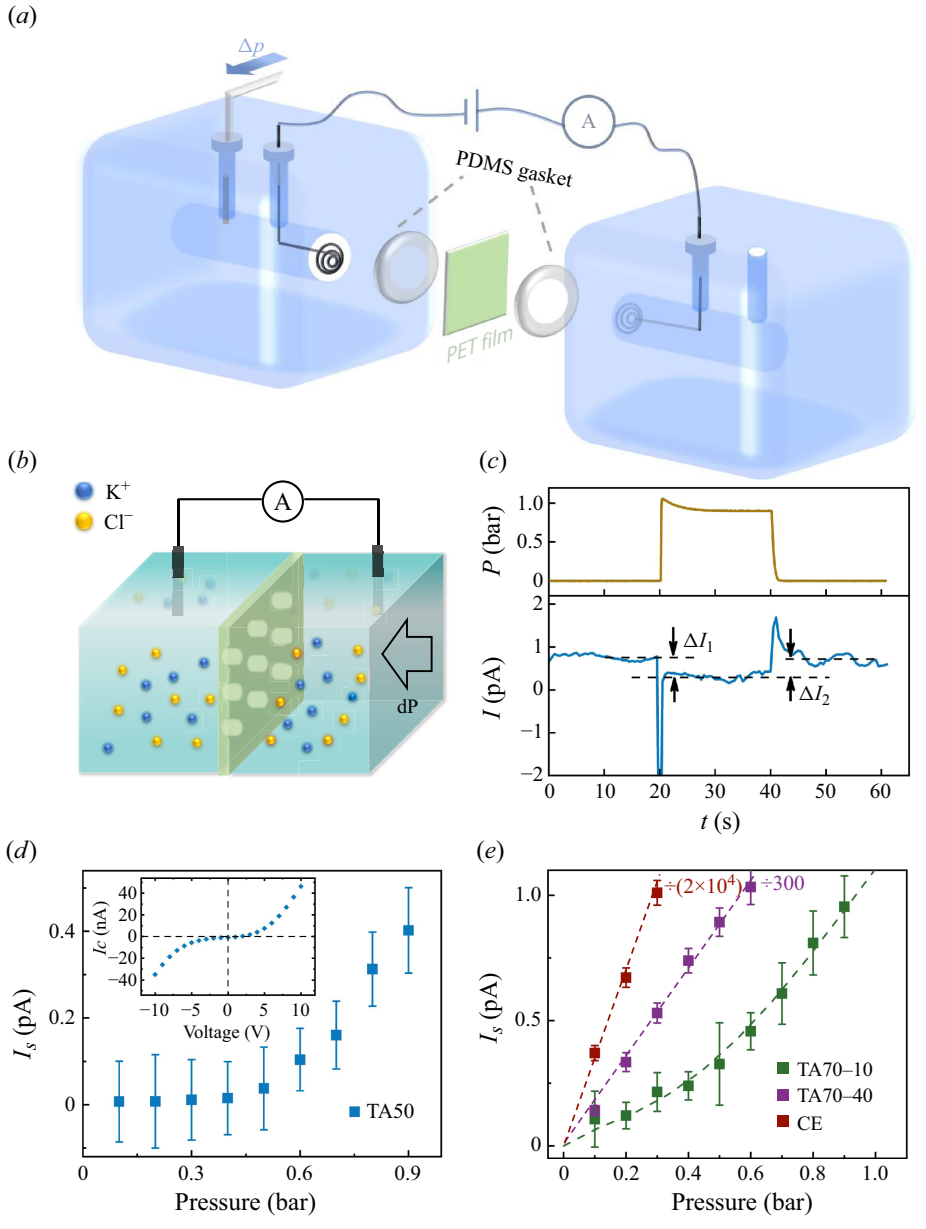


Figure 2. (*a*) Schematic diagram of the device for streaming current measurement. (*b*) Schematic description of ion transport across a PET membrane under an external pressure. (*c*) The current recordings (lower panel) when applied pressure (upper panel) was turned on. (*d*) The averaged streaming current exponentially increases with applied pressure in specimen TA50, with typical I–V curves in the inset that also show a strong nonlinear feature. (*e*) The streaming current gradually shows a linear response to the applied pressure as the channel radius grows. The current amplitudes of specimens TA70–40 and CE were divided by factors of 300 and 2×10^4, respectively, to make a comparison of the $\Delta p - I_s$ curves over a wide range of channel size.

We investigate the streaming current of annealed or chemically etched membranes with a wide range of diameters. The mean radius of specimen TA70−10, which was annealed at 70 °C for 10 min, is 0.4 nm derived from extrapolation of numerical fitting by TEM characterisation. Since the streaming current amplitude is proportional to the

https://doi.org/10.1017/jfm.2025.10336 Published online by Cambridge University Press

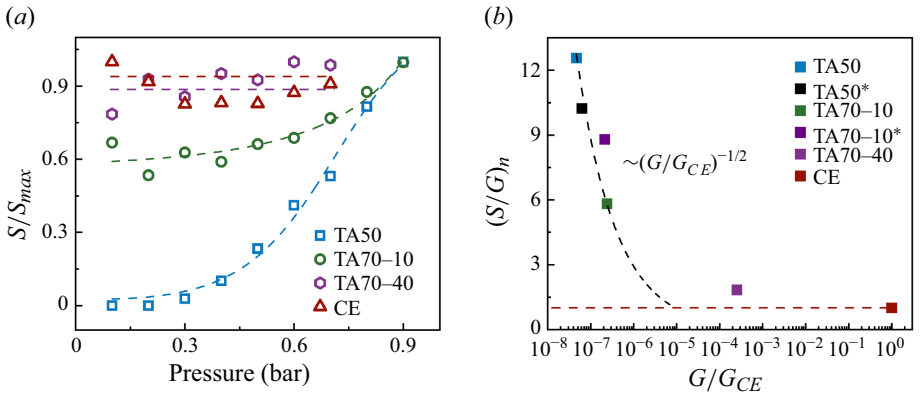


Figure 3. (*a*) The normalised streaming conductance (S/S_{max}) shows strong pressure dependency in angstrom channels and gradually becomes a constant as radius increases. (*b*) Normalised S/G versus normalised conductance for specimens across a wide range of radius. For small-size channels, the normalised S/G decreases with increasing normalised conductance $(S/G)_n \sim (G/G_{CE})^{-1/2}$, thus being inversely proportional to the radius $(S/G)_n \sim R^{-1}$.

channel cross-sectional area $I_s \sim R^2$, it is challenging to present data spanning a wide range of radii in a small current scale. To better represent the $\Delta p - I_s$ curve across a broad range of channel sizes, the streaming current amplitudes for specimens TA70–40 and CE (chemically etched) were reduced by factors of 300 and 2×10^4, respectively, as shown in figure 2(*e*). This normalisation enables a direct comparison of the linearity of the $\Delta p - I_s$ curve on the same scale. However, the streaming current still represents nonlinear features in specimen TA70−10, which is less obvious than specimen TA50. As D increases to 3.4 nm estimated from conductance measurement in specimen TA70−40, the nonlinear features disappear in both streaming current and ionic conduction (figure S2 of the supplementary material). As a control group, we measured the streaming current in specimen CE with a diameter of 220 nm (Apel *et al.* 2001; Mo *et al.* 2014). It shows a linear increase in I_s with Δp (figure 2*e*) with nearly a constant S, represented by purple symbols in figure 3(*a*).

To clearly demonstrate the transition of streaming conductance, we first calculated $S = I_s/\Delta p$ as a function of applied pressure and normalised the streaming conductance by the maximum value S_{max} at applied pressure from 0.7 to 0.9 bar as S/S_{max} for the four specimens shown in figure 3(*a*). For specimen TA50 with the smallest conductance and size, S presents an exponential rise in applied pressure that deviates from the existing knowledge of the electrokinetic theory approach. The rest of the angstrom-scale channels also showed such a nonlinear feature of the streaming current, although at different levels. We found S/S_{max} becomes less pressure-dependent as the channel size grows. When the mean radius $R > 2$ nm, we found the streaming conductance becomes independent of the applied pressure in specimens TA70−40 and CE. We could estimate the surface potential Φ from the streaming conductance divided by ionic conduction $S/G \sim \varepsilon_r \varepsilon_0 \Phi$, since it is still technically challenging to know the angstrom-channel size from both TEM characterisations and conduction measurement.

Here we normalised S/G by the value derived in specimen CE (220 nm in diameter), $(S/G)_n = (S/(S_{CE})) \cdot ((G_{CE})/G)$, where S_{CE} and G_{CE} are streaming conductance and conductance of specimen CE as shown in figure 3(*b*). The $(S/G)_n$ is inversely proportional to the square of normalised conductance G/G_{CE} for small channels. According to the HS equation, the surface potential ought to be independent of channel size; however, our

https://doi.org/10.1017/jfm.2025.10336 Published online by Cambridge University Press

results showed that Φ increases as the channel narrows, as we discuss later. Additional data for specimens TA50 and TA70−10 are included in figure 3(*b*), with the original data found in figure S3 of the supplementary material.

We attributed the pressure-dependent streaming conductance to the strong Coulomb interaction between counterions and the carboxyl groups on the surface of latent-track channels (Wang *et al.* 2018), where the Coulomb interaction can be reinforced in 1-D angstrom channels according to previous studies (Teber 2005; Kavokine *et al.* 2019). Pressure-driven flow within the channels gives hydrodynamic friction to the bound counterions, increasing their probability of releasing surface charge and thus forming the streaming current. We can approximate the streaming current by Kramer's escape problem with a potential well, considering the counterion transport as the summation of a mean first passage time τ_m escaping from the potential well and the time of free drifting τ_d. Thus, we have the streaming current as $I_s = N\Sigma A/(\tau_m + \tau_d)$, where Σ, N, A and L are surface charge density, number of parallel channels, inner wall surface area of nanochannels $A = 2\pi RL$ and channel length. Time τ_m can be approximated in a form of $\tau_m \sim \mathrm{e}^{\Delta U_s - c\Delta p}$, where ΔU_s is the Coulomb interaction energy normalised by k_BT and c is a friction coefficient for the counterions normalised by k_BT. At a steady state, the pressure-driven force equals the friction, $2\pi R\lambda L v_w = \Delta p \cdot \pi R^2$, where λ is the friction coefficient including the entrance effects and v_w is flow velocity. Thus, we have the time of free drifting as $\tau_d = 2\lambda L^2/(\Delta pR)$. Finally, we have the streaming current in 1-D heterogeneously charged angstrom channels expressed as follows:

$$j_s \sim \frac{2NL\Sigma/R}{\tau_m^0 \mathrm{e}^{\Delta U_s - c\Delta p} + 2\lambda L^2/(\Delta pR)}, \tag{3.1}$$

where τ_m^0 is the mean first passage time in the limit $\Delta U_s \to 0$. Here we can define a Damköhler number $Da = \tau_d/\tau_m$ to indicate the ratio between the drifting (residence) time of counterion transport through the channel $\tau_d = 2\lambda L^2/(\Delta pR)$ and the mean first passage time $\tau_m = \tau_m^0 \mathrm{e}^{\Delta U_s - c\Delta p}$ which describes the dissociation of counterions from the surface charge that can be considered as a chemical reaction. Thus, we can rewrite the equation of streaming current as follows:

$$I_s \sim \left[\frac{Da}{1+Da}\frac{\pi N \Sigma R^2}{\lambda}\right]\frac{\Delta p}{L}, \tag{3.2}$$

where the factor in square bracket is the Onsager reciprocal coefficient. Thus, we can derive the S/G according to the form of streaming current in the form of the HS equation:

$$S/G \sim \varepsilon_r\varepsilon_0\Phi \sim \frac{Da}{1+Da}\cdot \Sigma b, \tag{3.3}$$

where b, ε_r and ε_0 are slip length, relative permittivity of water and vacuum permittivity. Given the challenges in obtaining details such as Coulomb interactions ΔU_s and flow velocity in our polymer angstrom-scale channels, we calculate the dimensionless coefficient using a unitless contour map as a function of applied pressure and channel radii. We first examine the effects of applied pressure on Da and streaming conductance. For small Da when $\tau_d/\tau_m \ll 1$, we have $Da/(1+Da) \approx Da$, and the streaming conductance is proportional to $Da \sim \mathrm{e}^{-\Delta U_s + c\Delta p}/R\Delta p$. This results in an exponential increase of streaming conductance with the applied pressure $S \sim \mathrm{e}^{-\Delta U_s + c\Delta p}$ by (3.2). But, as Δp exceeds a threshold value, large Da leading to $Da/(1+Da) \sim 1$, the streaming conductance reaches a constant value, as shown in figure 4(*c*) for high Δp.

Now we focus on the size effects. As channel radius increases, the Coulomb interaction between counterions and surface decreases $\Delta U_s \sim R^{-1}$ due to the reinforced Coulomb

https://doi.org/10.1017/jfm.2025.10336 Published online by Cambridge University Press

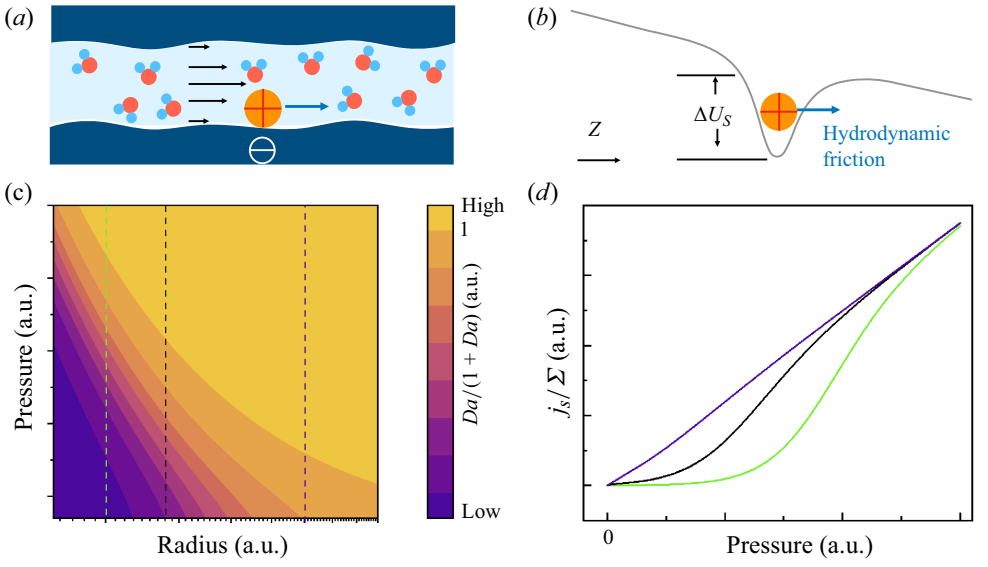


Figure 4. (*a*) Scheme of molecular streaming with a counterion (yellow) strongly bound to surface charge (white), causing pressure-dependent streaming current. (*b*) The thermal dynamics process of bound ions under the action of hydrodynamic friction can be described by the 1-D Kramer escape problem from a Coulomb potential well. (*c*) The dimensionless coefficient $Da/(Da+1)$ describes the nonlinearity of streaming current as functions of applied pressure and channel radius. The yellow region indicates constant streaming conductance zone. (*d*) The streaming current flux normalised by surface charge density (j_s/Σ) as a function of applied pressure in channels of three different sizes, where the colour corresponds to the dashed lines in (*c*).

interaction and large Bjerrum length in confinement, as reported by Teber (2005) and Kavokine *et al.* (2019). The reduced Coulomb interaction ΔU_s in large channels increases Da thus leading to $Da/(1+Da)\sim 1$ for a linear $I_s-\Delta p$ curve shown as a purple solid line in figure 4(*d*). In such a case, the streaming conductance becomes a constant. We assume a constant number of binding sites across channels of different sizes, rather than a constant surface charge density, as the binding sites are generated during irradiation instead of the annealing process, even though the channel size gradually increases with annealing. Thereby, we have the surface charge density inversely proportional to R, $\Sigma = ne/2\pi RL \sim R^{-1}$, where n is the number of charged sites as a constant. Thus, S/G for large Da is inversely proportional to the channel radius $(S/G)_n \sim \Sigma \sim R^{-1}$. Previous results (Fumagalli *et al.* 2018) showed that the permittivity of a water channel ε_r decreases as the channel radius becomes of angstrom scale, so we suspect that the surface potential Φ possibly also increases as the channel size decreases, which well explains the anomalous increases of surface potential in angstrom-scale channels.

Although directly observing ionic transport and detailing ion–wall interactions remain challenging, we believe our findings provide new insights into electrokinetic phenomena in angstrom channels where the concept of the electric double layer fails. We found that the streaming current can only be activated when applied pressure exceeds a threshold value, which was only observed in a voltage-gated carbon nanotube (Marcotte *et al.* 2020) although with a different tendency. Our results reveal electrokinetic phenomena when the channel size gets close to an atomically thin Helmholtz layer, which also provide evidence of the counterion-correlated blockade of ionic transport in confinement.

https://doi.org/10.1017/jfm.2025.10336 Published online by Cambridge University Press

A generic external force, including electrical force and hydrodynamic friction force, could release the counterions, forming the ionic current.

Our results with increasing channel radius give a threshold boundary from subcontinuum to continuum transport of $\sim$2 nm, above which size the ionic transport reaches a regime where flux is linearly proportional to the generic force. In such a subcontinuum regime, when the electric double-layer concept fails, the reciprocal factor between water flow and ionic fluxes needs to be reproduced. For instance, although we derived the reciprocal factor in the form of effective surface potential from streaming current, the fluxes of mass transport are no longer a linear summation of the fluxes driven by individual forces, as the fluxes may exponentially respond to a generic force. When $\Delta U_s/k_BT > 1$, a threshold pressure is required to activate the streaming current, as described by (3.1). The Coulomb interaction is significantly enhanced in angstrom-scale confinement due to the reduced permittivity, which increases the Bjerrum length of water in confinement. When $\Delta U_s/k_BT < 1$, thermodynamic energy enables the counterions to dissociate from the surface charge, induces a negligible $\Delta U_s/k_BT$ term, simplifying (3.1) into the conventional HS equation, where no threshold pressure is needed for streaming current generation.

Previous studies have attributed nonlinear ionic transport in angstrom-scale channels to dehydration and self-energy barriers, particularly under voltage-driven conditions (Zhang, Kamenev & Shklovskii 2005; Zwolak *et al.* 2009; Feng *et al.* 2016). However, pressure-driven transport shows distinct behaviour – nonlinear streaming currents have not been reported in bare channels, to our knowledge, although the ions also need to overcome the dehydration/self-energy barrier in other types of angstrom-scale channels (Mouterde *et al.* 2019; Marcotte *et al.* 2020). We attribute the nonlinearity observed in our system to heterogeneous surface charges, arising from Coulomb interactions between counterions and discrete surface sites. However, the behaviour of ions and water near the surface is quite complicated, which requires further understanding of the surface interactions. Our work probably gives information on the Donnan potential of a dielectric surface through an experimental approach to streaming current. It is still challenging to characterise the water flows and mass transport on such a small scale in polymer channels, but our work may help in understanding something of the flow and transport in confinement. The strong ion–wall interaction will be critical for ionic diffusion and transport in dielectric angstrom-scale channels and may be useful in ionic separation and energy applications.

4. Conclusions

We report pressure-dependent streaming conductance in heterogeneously charged latent-track angstrom-scale channels, which contradicts existing knowledge based on the electrical double-layer theories that the streaming conductance is pressure-independent. To investigate the size effects, we developed the channel size from the angstrom scale to a few nanometres by thermal annealing in a water bath and characterised it by staining under TEM. As the channel radius increases above $\sim$2 nm, the streaming conductance gradually becomes constant, as predicted by the PNP and HS equations.

We derived the anomalously effective surface potential increasing as the channel narrows by dividing streaming conductance by conduction, which we attribute to the increase in surface charge density with decreasing channel size in angstrom channels. Our hypothesis attributed the pressure-dependent streaming conductance to the strong interaction between counterions and surface charge, where the increase of applied pressure increases the friction force on the bound cations and the probability of release from the surface, thus forming a current. The Coulomb interaction decreased with an increase in channel radius, resulting in a constant streaming conductance.

https://doi.org/10.1017/jfm.2025.10336 Published online by Cambridge University Press

We quantitatively approximated the ionic transport using the 1-D Kramer escape theory framework, which well explained the pressure-dependent streaming conductance with the impacts of size effects. We derived a phase diagram of dimensionless coefficient $Da/(Da+1)$ based on Damköhler number, which can distinguish between pressure-dependent and pressure-independent regimes as functions of radius and pressure gradient. We discovered pressure-dependent streaming current in heterogeneously charged angstrom channels, where surfaces are charged via deprotonation or physical adsorption processes for dielectric surfaces. Our work is helpful for understanding ionic transport in confinement and may be useful for energy applications and ion separations.

Supplementary material. Supplementary material is available at https://doi.org/10.1017/jfm.2025.10336.

Acknowledgements. The authors thank Professor J. Liu and Professor J. Duan at HIRFL for their help with film irradiation and useful discussions concerning the RuO_4 staining TEM characterisation, and the anonymous reviewers for their valuable feedback and suggestions.

Funding. This work was supported by the National Natural Science Foundation of China (nos. 12388101, 12241201, 12075191) and the Fundamental Research Funds for the Central Universities with grant no. D5000210626.

Declaration of interests. The authors report no conflict of interest.

References

Adla, A., Fuess, H. & Trautmann, C. 2003 Characterization of heavy ion tracks in polymers by transmission electron microscopy. *J. Polymer Sci. Part B: Polymer Phys.* **41** (22), 2892–2901.

Alkhadra, M.A., *et al.* 2022 Electrochemical methods for water purification, ion separations, and energy conversion. *Chem. Rev.* **122** (16), 13547–13635.

Aluru, N.R., *et al.* 2023 Fluids and electrolytes under confinement in single-digit nanopores. *Chem. Rev.* **123** (6), 2737–2831.

Apel, P.Yu, Korchev, YuE., Siwy, Z., Spohr, R. & Yoshida, M. 2001 Diode-like single-ion track membrane prepared by electro-stopping. *Nuclear Instrum. Meth. Phys. Res. B* **184** (3), 337–346.

Apel, P.Yu, Blonskaya, I.V., Ivanov, O.M., Kristavchuk, O.V., Nechaev, A.N., Olejniczak, K., Orelovich, O.L., Polezhaeva, O.A. & Dmitriev, S.N. 2022 Do the soft-etched and UV-track membranes actually have uniform cylindrical subnanometer channels? *Radiat. Phys. Chem.* **198**, 110266.

Bazant, M.Z. &Squires, T.M. 2004 Induced-charge electrokinetic phenomena: theory and microfluidic applications. *Phys. Rev. Lett.* **92** (6), 066101.

Bazant, M.Z. & Squires, T.M. 2010 Induced-charge electrokinetic phenomena. *Curr. Opin. Colloid Interface Sci.* **15** (3), 203–213.

Behrens, S.H. & Grier, D.G. 2001 The charge of glass and silica surfaces. *J. Chem. Phys.* **115** (14), 6716–6721.

Bocquet, L. & Charlaix, E. 2010 Nanofluidics, from bulk to interfaces. *Chem. Soc. Rev.* **39** (3), 1073–1095.

Bonthuis, D.J. & Netz, R.R. 2012 Unraveling the combined effects of dielectric and viscosity profiles on surface capacitance, electro-osmotic mobility, and electric surface conductivity. *Langmuir* **28** (46), 16049–16059.

Cao, Y., Zhou, W., Shen, C., Qiu, H. & Guo, W. 2024 Proton coulomb blockade effect involving covalent oxygen-hydrogen bond switching. *Phys. Rev. Lett.* **132** (18), 188401.

Catalano, J. & Bentien, A. 2014 Influence of temperature on the electrokinetic properties and power generation efficiency of nafion® 117 membranes. *J. Power Sources* **262**, 192–200.

Delgado, Á.V., González-Caballero, F., Hunter, R.J., Koopal, L.K. & Lyklema, J. 2007 Measurement and interpretation of electrokinetic phenomena. *J. Colloid Interface Sci.* **309** (2), 194–224.

Emmerich, T., Vasu, K.S., Niguès, A., Keerthi, A., Radha, B., Siria, A. & Bocquet, L. 2022 Enhanced nanofluidic transport in activated carbon nanoconduits. *Nat. Mater.* **21** (6), 696–702.

Esfandiar, A., Radha, B., Wang, F.C., Yang, Q., Hu, S., Garaj, S., Nair, R.R., Geim, A.K. & Gopinadhan, K. 2017 Size effect in ion transport through angstrom-scale slits. *Science* **358** (6362), 511–513.

https://doi.org/10.1017/jfm.2025.10336 Published online by Cambridge University Press

FAUCHER, S., *et al.* 2019 Critical knowledge gaps in mass transport through single-digit nanopores: a review and perspective. *J. Phys. Chem. C* **123** (35), 21309–21326.

FENG, J., LIU, K., GRAF, M., DUMCENCO, D., KIS, A., DI VENTRA, M. & RADENOVIC, A. 2016 Observation of ionic Coulomb blockade in nanopores. *Nat. Mater.* **15** (8), 850–855.

FUMAGALLI, L., *et al.* 2018 Anomalously low dielectric constant of confined water. *Science* **360** (6395), 1339–1342.

GILLESPIE, D. 2012 High energy conversion efficiency in nanofluidic channels. *Nano Lett.* **12** (3), 1410–1416.

GILLESPIE, D., KHAIR, A.S., BARDHAN, J.P. & PENNATHUR, S. 2011 Efficiently accounting for ion correlations in electrokinetic nanofluidic devices using density functional theory. *J. Colloid Interface Sci.* **359** (2), 520–529.

GUO, Z., LI, F., WU, X., LIANG, Z., JUNAID, M., XIE, J., LU, L., DUAN, J., LIU, J. & YAO, H. 2024 Efficient ion sieving and ion transport properties in sub-nanoporous polyetherimide membranes. *Desalination* **573**, 117192.

HARTKAMP, R., BIANCE, A.-L., FU, L., DUFRÊCHE, J.F., BONHOMME, O., JOLY, L. 2018 Measuring surface charge: why experimental characterization and molecular modeling should be coupled. *Curr. Opin. Colloid In* **37**, 101–114.

VAN DER HEYDEN, F.H.J., STEIN, D., BESTEMAN, K., LEMAY, S.G. & DEKKER, C. 2006 Charge inversion at high ionic strength studied by streaming currents. *Phys. Rev. Lett.* **96** (22), 224502.

VAN DER HEYDEN, F.H.J., STEIN, D. & DEKKER, C. 2005 Streaming currents in a single nanofluidic channel. *Phys. Rev. Lett.* **95** (11), 116104.

HOLT, J.K., PARK, H.G., WANG, Y., STADERMANN, M., ARTYUKHIN, A.B., GRIGOROPOULOS, C.P., NOY, A. & BAKAJIN, O. 2006 Fast mass transport through sub-2-nanometer carbon nanotubes. *Science* **312** (5776), 1034–1037.

ITOH, Y., *et al.* 2022 Ultrafast water permeation through nanochannels with a densely fluorous interior surface. *Science* **376** (6594), 738–743.

KAVOKINE, N., BOCQUET, M.-L. & BOCQUET, L. 2022 Fluctuation-induced quantum friction in nanoscale water flows. *Nature* **602** (7895), 84–90.

KAVOKINE, N., MARBACH, S., SIRIA, A., BOCQUET, L. 2019 Ionic Coulomb blockade as a fractional Wien effect. *Nat. Nanotechnol.* **14** (6), 573–578.

KEERTHI, A., GOUTHAM, S., YOU, Y., IAMPRASERTKUN, P., DRYFE, R.A.W., GEIM, A.K. & RADHA, B. 2021 Water friction in nanofluidic channels made from two-dimensional crystals. *Nat. Commun.* **12** (1), 3092.

KIM, Y.W. & NETZ, R.R. 2006 Electro-osmosis at inhomogeneous charged surfaces: hydrodynamic versus electric friction. *J. Chem. Phys.* **124** (11), 114709.

LI, X., *et al.* 2019 Fast and selective fluoride ion conduction in sub-1-nanometer metal-organic framework channels. *Nat. Commun.* **10** (1), 2490.

LI, Z., MISRA, R.P., LI, Y., YAO, Y.-C., ZHAO, S., ZHANG, Y., CHEN, Y., BLANKSCHTEIN, D. & NOY, A. 2023 Breakdown of the Nernst–Einstein relation in carbon nanotube porins. *Nat. Nanotechnol.* **18** (2), 177–183.

LYKLEMA, J. 2003 Electrokinetics after smoluchowski. *Colloids Surf. A: Physicochem. Engng Aspects* **222** (1–3), 5–14.

MARCOTTE, A., MOUTERDE, T., NIGUÈS, A., SIRIA, A. & BOCQUET, L. 2020 Mechanically activated ionic transport across single-digit carbon nanotubes. *Nat. Mater.* **19** (10), 1057–1061.

MCELDREW, M., GOODWIN, Z.A.H., KORNYSHEV, A.A. & BAZANT, M.Z. 2018 Theory of the double layer in water-in-salt electrolytes. *J. Phys. Chem. Lett.* **9** (19), 5840–5846.

MO, D., LIU, J.D., DUAN, J.L., YAO, H.J., LATIF, H., CAO, D.L., CHEN, Y.H., ZHANG, S.X., ZHAI, P.F. & LIU, J. 2014 Fabrication of different pore shapes by multi-step etching technique in ion-irradiated PET membranes. *Nuclear Instrum. Meth. Phys. Res. B* **333**, 58–63.

MOUTERDE, T., KEERTHI, A., POGGIOLI, A.R., DAR, S.A., SIRIA, A., GEIM, A.K., BOCQUET, L. & RADHA, B. 2019 Molecular streaming and its voltage control in Ångström-scale channels. *Nature* **567** (7746), 87–90.

NOSKOV, S.Y., BERNECHE, S. & ROUX, B. 2004 Control of ion selectivity in potassium channels by electrostatic and dynamic properties of carbonyl ligands. *Nature* **431** (7010), 830–834.

OLTHUIS, W., SCHIPPERS, B., EIJKEL, J. & VAN DEN BERG, A. 2005 Energy from streaming current and potential. *Sensors Actuators B: Chemical* **111**, 385–389.

ØSTEDGAARD-MUNCK, D.N., CATALANO, J., KRISTENSEN, M.B. & BENTIEN, A. 2017 Membrane-based electrokinetic energy conversion. *Mater. Today Energy* **5**, 118–125.

RADHA, B., *et al.* 2016 Molecular transport through capillaries made with atomic-scale precision. *Nature* **538** (7624), 222–225.

https://doi.org/10.1017/jfm.2025.10336 Published online by Cambridge University Press

ROBIN, P., *et al.* 2023 Long-term memory and synapse-like dynamics in two-dimensional nanofluidic channels. *Science* **379** (6628), 161–167.

ROBIN, P., KAVOKINE, N. & BOCQUET, L. 2021 Modeling of emergent memory and voltage spiking in ionic transport through Angstrom-scale slits. *Science* **373** (6555), 687–691.

SCHAURIES, D., MOTA-SANTIAGO, P., GILBERT, E.P., KIRBY, N., TRAUTMANN, C. & KLUTH, P. 2018 Structure, morphology and annealing behavior of ion tracks in polycarbonate. *Eur. Polym. J.* **108**, 406–411.

SHI, D., WANG, W., LIANG, Y., DUAN, L., DU, G. & XIE, Y. 2023 Ultralow energy consumption Angstrom-fluidic memristor. *Nano Lett.* **23** (24), 11662–11668.

SIRIA, A., PONCHARAL, P., BIANCE, A.-L., FULCRAND, RÉMY, BLASE, X., PURCELL, S.T. & BOCQUET, L. 2013 Giant osmotic energy conversion measured in a single transmembrane boron nitride nanotube. *Nature* **494** (7438), 455–458.

STOREY, B.D. & BAZANT, M.Z. 2012 Effects of electrostatic correlations on electrokinetic phenomena. *Phys. Rev. E–Stat., Nonlinear Soft Matter Phys.* **86** (5), 056303.

TAN, R., *et al.* 2020 Hydrophilic microporous membranes for selective ion separation and flow-battery energy storage. *Nat. Mater.* **19** (2), 195–202.

TEBER, S. 2005 Translocation energy of ions in nano-channels of cell membranes. *J. Stat. Mech.: Theory Exp.* **2005** (07), P07001–P07001.

WANG, L., BOUTILIER, M.S.H., KIDAMBI, P.R., JANG, D., HADJICONSTANTINOU, N.G. & KARNIK, R. 2017 Fundamental transport mechanisms, fabrication and potential applications of nanoporous atomically thin membranes. *Nat. Nanotechnol.* **12** (6), 509–522.

WANG, P., *et al.* 2018 Ultrafast ion sieving using nanoporous polymeric membranes. *Nat. Commun.* **9** (1), 569.

WEN, Q., *et al.* 2016 Highly selective ionic transport through subnanometer pores in polymer films. *Adv. Funct. Mater.* **26** (32), 5796–5803.

WERNER, C., ZIMMERMANN, R. & KRATZMÜLLER, T. 2001 Streaming potential and streaming current measurements at planar solid/liquid interfaces for simultaneous determination of zeta potential and surface conductivity. *Colloids Surf. A: Physicochem. Engng Aspects* **192** (1–3), 205–213.

XIE, Y., FU, L., NIEHAUS, T. & JOLY, L. 2020 Liquid-solid slip on charged walls: the dramatic impact of charge distribution. *Phys. Rev. Lett.* **125** (1), 014501.

XIE, Y., SHI, D., WANG, W. & WANG, Z. 2023 Surface-charge governed ionic blockade in Angstrom-scale latent-track channels. *Nanoscale* **15** (21), 9560–9566.

XU, D., YAN, M. & XIE, Y. 2024 Energy harvesting from water streaming at charged surface. *Electrophoresis* **45** (3–4), 244–265.

XUE, G., *et al.* 2017 Water-evaporation-induced electricity with nanostructured carbon materials. *Nat. Nanotechnol.* **12** (4), 317–321.

XUE, S., YEH, L.-H., MA, Y. & QIAN, S. 2014 Tunable streaming current in a pH-regulated nanochannel by a field effect transistor. *J. Phys. Chem. C* **118** (12), 6090–6099.

YANG, G., QIAN, Y., LIU, D., WANG, L., MA, Y., SUN, J., SU, Y., JARVIS, K., WANG, X. & LEI, W. 2022 Simultaneous electrokinetic energy conversion and organic molecular sieving by two-dimensional confined nanochannels. *Chem. Engng J.* **446**, 136870.

YAROSHCHUK, A. & LUXBACHER, T. 2010 Interpretation of electrokinetic measurements with porous films: role of electric conductance and streaming current within porous structure. *Langmuir* **26** (13), 10882–10889.

ZHANG, J., KAMENEV, A. & SHKLOVSKII, B.I. 2005 Conductance of ion channels and nanopores with charged walls: a toy model. *Phys. Rev. Lett.* **95** (14), 148101.

ZHOU, W., GUO, Y., ZHANG, Z., GUO, W. & QIU, H. 2023 Field-induced hydration shell reorganization enables electro-osmotic flow in nanochannels. *Phys. Rev. Lett.* **130** (8), 084001.

ZIMMERMANN, R., DUKHIN, S. & WERNER, C. 2001 Electrokinetic measurements reveal interfacial charge at polymer films caused by simple electrolyte ions. *J. Phys. Chem. B* **105** (36), 8544–8549.

ZWOLAK, M., LAGERQVIST, J. & DI VENTRA, M. 2009 Quantized ionic conductance in nanopores. *Phys. Rev. Lett.* **103** (12), 128102.

https://doi.org/10.1017/jfm.2025.10336 Published online by Cambridge University Press